Bio-Derived Active Packaging: Genipin-Cross-Linked Chitosan/Cellulose Nanocrystal Films Embedded with Lemongrass Essential Oil for Extended Post-Harvest Fruit Life

Yu Lin,[a] Di Wu,[a] Xinyu Xu,[a] Guiyuan Zhao,[b] Baoying Shi,[c,*] Yufeng Wang,[a,*] and Haiyan Song [a,*]

** Corresponding author: sby1980@126.com (B. Shi), ppcwyf@tust.edu.cn (Y. Wang), hysong@tust.edu.cn (H. Song)*

DOI: 10.15376/biores.21.2.5205-5227

GRAPHICAL ABSTRACT

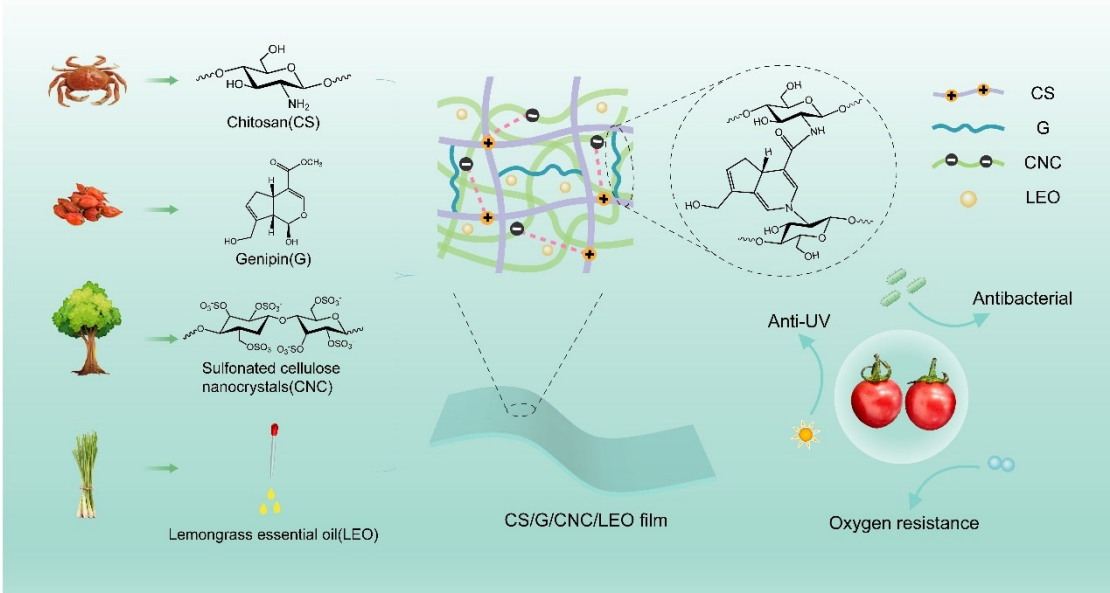

Bio-Derived Active Packaging: Genipin-Cross-Linked Chitosan/Cellulose Nanocrystal Films Embedded with Lemongrass Essential Oil for Extended Post-Harvest Fruit Life

Yu Lin,[a] Di Wu,[a] Xinyu Xu,[a] Guiyuan Zhao,[b] Baoying Shi,[c,]* Yufeng Wang,[a,]* and Haiyan Song [a,]*

Chitosan-based films are attractive eco-friendly substitutes for petrochemical packaging; however, their commercialization is limited by modest mechanical strength and limited functionality. This study presents a fully bio-sourced composite in which chitosan is covalently cross-linked with the natural reagent genipin, nano-reinforced with sulfonated cellulose nanocrystals (CNCs) and functionalized with lemongrass essential oil (LEO) as a broad-spectrum antimicrobial. Spectroscopic, microscopic, and thermal analyses confirmed the formation of a densely reticulated architecture through Schiff-base chemistry and hydrogen bonding. The optimized CS/G/CNC/LEO film reached a tensile strength of 49 MPa (above 80% higher than pure chitosan), showed a 74% fall in swelling ratio, and exhibited superior O_2 and UV barriers. As a coating for cherry tomatoes, the material restricted weight loss to 9%, preserved firmness, titratable acidity and vitamin C, suppressed microbial growth and respiration, and prolonged post-harvest shelf life by six days under room temperature storage conditions. These results demonstrate the potential of CS/G/CNC/LEO films as a sustainable active food packaging material.

DOI: 10.15376/biores.21.2.5205-5227

Keywords: Chitosan; Genipin cross-linking; Sulfonated cellulose nanocrystals; Lemongrass essential oil; Active bio-composite film; Sustainable food packaging

Contact information: a: State Key Laboratory of Bio-based Fiber Materials, Tianjin University of Science and Technology, Tianjin 300457, China; b: Tianjin Baide Paper Co., LTD, Tianjin 300382, China; c: Tianjin Tianshi College, Tianjin 301700, China;
** Corresponding author: ppcwyf@tust.edu.cn (Y. Wang), hysong@tust.edu.cn (H. Song)*

INTRODUCTION

Postharvest losses of fresh fruits and vegetables remain severe worldwide. This problem is primarily attributed to the rapid physiological changes that occur after harvest, and any disruption in the cold-chain logistics system often further exacerbates this phenomenon. Such losses not only impose a substantial economic burden but also lead to significant waste of valuable nutritional resources (Liu *et al*. 2020; Zhang *et al*. 2023). For decades, petroleum-based plastics have dominated the field of food packaging due to their excellent barrier and mechanical properties. However, their environmental persistence and their role as a major source of microplastic pollution have made the development of sustainable and environmentally friendly alternatives an urgent priority.

In this context, chitosan, a biopolymer derived from chitin, has been widely regarded as a highly promising candidate material. Chitosan consists of D-glucosamine

and N-acetyl-D-glucosamine units linked by β-(1-4) glycosidic bonds. It is well known for its biodegradability, biocompatibility, and intrinsic antimicrobial activity (Poznanski *et al*. 2023). These characteristics make it an ideal material for constructing "active" packaging systems designed to extend the shelf life of perishable foods while reducing reliance on synthetic polymers (Deng *et al*. 2012; Kaewklin *et al*. 2018; Reesha *et al*. 2015). Nevertheless, the widespread application of pure chitosan films remains limited because of their relatively low tensile strength and high hydrophilicity (Huang *et al*. 2012; Yu *et al*. 2023).

To overcome these limitations, two main strategies are commonly used, including chemical crosslinking and nanofiller reinforcement. Chemical crosslinking can make the polysaccharide network more compact and improve its mechanical strength (Akhtar and Ding, 2017). However, synthetic crosslinking agents such as formaldehyde (Tashta *et al*. 2021) and glutaraldehyde (Pereira *et al*. 2020) show cytotoxicity, which limits their application in food-contact materials (Dustad *et al*. 2022; Ko *et al*. 2024). Genipin, a natural compound derived from *Gardenia jasminoides*, provides a safer and more environmentally friendly alternative. It reacts with the amino groups of chitosan through nucleophilic attack, leading to ring opening and subsequent rearrangement reactions that form stable network structure with chitosan. This reaction also produces a characteristic blue color and results in a matrix with improved strength and lower solubility (Khan *et al*. 2014; Xie *et al*. 2023; Ahmad *et al*. 2024).

In addition to chemical crosslinking, the use of high aspect ratio nanofillers for physical reinforcement is another effective method to improve film performance. Sulfonated cellulose nanocrystals have attracted attention due to their high crystallinity, large surface area, abundant hydroxyl groups, and natural renewability and biodegradability. Compared with unmodified cellulose nanocrystals, sulfonation improves their water dispersibility and increases electrostatic repulsion, which leads to better dispersion and stability in aqueous systems (Sajjadi *et al.* 2024; Sun *et al.* 2025). Their large surface area and hydrophilic nature also support good compatibility with the polymer matrix and help form stable composite structures. When added to the chitosan matrix, they form strong hydrogen bonding and electrostatic interactions, which improve tensile strength, reduce gas permeability, and enhance the microstructure of the films (Gan *et al.* 2021; Babaei-Ghazvini *et al*. 2022).

However, sulfonation treatment may raise concerns about food safety. In fact, sulfonic groups and their derivatives are widely found in nature, and their safety has been reported in many natural systems. For example, sulfonated polysaccharides are widely present in marine algae and are also found in mammals and invertebrates (Mourao and Pereira 1999). At present, these materials are widely used in the food, cosmetic, and pharmaceutical industries (Wijesekara *et al*. 2011). Recent studies show that sulfonated polysaccharides play an important role in human health and nutrition (Kalita *et al*. 2025; Zhang *et al*. 2025). In addition, sulfonic and sulfate groups have been reported to show beneficial biological effects, including roles in bone repair and regeneration (Wang *et al*. 2025). These findings support the evaluation of the safety of sulfonation modification and suggest that sulfonated structures do not inherently pose risks, but their safety depends on the specific chemical environment and application conditions. In summary, current evidence suggests that sulfonated CNC is a promising candidate for food contact materials. However, to ensure the safety of its application, further in-depth studies on migration behavior and long-term exposure effects are required.

In addition to structural integrity, active packaging for fresh produce also requires effective antibacterial properties. Plant-derived essential oils (EOs), which are complex blends of volatile terpenoids and phenolics, provide broad-spectrum antibacterial, antifungal and antioxidant activities and are generally recognized as safe (GRAS) (Adukwu *et al*. 2016; de Souza *et al*. 2020; Rabbani *et al*. 2026). Among them, lemongrass oil (LEO, *Cymbopogon* spp.) has clear advantages due to its high citral content, which can disrupt microbial cell membranes and respiratory enzymes and lead to rapid cell death (Mohd Daud *et al*. 2026). Films incorporating lemongrass oil have attracted considerable attention as sustainable packaging materials, and numerous studies have demonstrated their effectiveness in food preservation. Ahmad *et al*. (2026) developed an edible composite coating based on lemongrass oil and carboxymethyl cellulose for fresh chicken stored at 4 °C. This coating effectively reduced total volatile basic nitrogen (TVB-N) levels, delayed color deterioration, and minimized water loss. Wu *et al*. (2026) fabricated Zein/Gly/TA/SA/LEO films by crosslinking corn zein with tannic acid and incorporating lemongrass oil. The resulting films exhibited enhanced surface hydrophobicity, improved ultraviolet-blocking properties, and antibacterial activity against *Escherichia coli* and *Staphylococcus aureus*, thereby extending the shelf life of cherry tomatoes to 11 days. de Albuquerque Sousa *et al*. (2026) developed an oat starch cryogel incorporating lemongrass oil for strawberries stored at 4 °C. This system reduced weight loss to 0.57% and spoilage to 5.26%, while maintaining titratable acidity (0.97%), soluble solids (6.9 °Brix), and firmness (1.21 N) for up to 15 days.

Despite these individual advances, the development of an integrated packaging system that combines improved mechanical strength, excellent biocompatibility, and broad-spectrum antimicrobial activity remains challenging. Most existing studies have focused on a single modification strategy, and there is limited research on the combined effects of using a natural crosslinker, a bio-based nanomaterial, and an antimicrobial agent within a chitosan matrix.

This study investigated the preparation of a multifunctional CS film that is crosslinked with genipin, nano-reinforced with sulfonated CNCs, and loaded with LEO. This design is expected to improve mechanical and barrier properties through combined chemical and physical interactions and to provide sustained antimicrobial activity through controlled release of LEO, without the use of synthetic additives. The prepared CS/G/CNC/LEO films were characterized, and their effectiveness was evaluated using a cherry tomato preservation model. However, the safety of composite materials has not yet been studied. Therefore, this study provides a scalable approach that can be used to develop the next generation of active packaging for fresh agricultural products.

EXPERIMENTAL

Materials

Chitosan (degree of deacetylation ≥95%, viscosity 100–200 mPa·s, M_w = 60 to 75 kDa), glacial acetic acid (≥99%), and genipin (G, ≥98%) were supplied by Shanghai Aladdin Biochemical Technology Co., Ltd. (Shanghai, China). Sulfonated cellulose nanocrystals (CNC-S, 8wt%) were provided by Guilin Qihong Technology Co., Ltd. (Guilin, China). Food-grade lemongrass essential oil (LEO, ≥99%) was obtained from Aromatec Inc. (Shenzhen, China). Tween 80 (polysorbate 80, ≥99%) was purchased from Macklin Biochemical Co., Ltd. (Shanghai, China). All other reagents were of analytical

grade and used without further purification. De-ionised water (18.2 MΩ cm) was employed throughout.

Preparation of the CS/G/CNC/LEO Films

The preparation of the composite films is illustrated in Fig. 1. A lemongrass essential oil (LEO) emulsion was first prepared by adding 0.2 g of polysorbate 80 and 0.1 g of LEO into 10 mL of deionized water, followed by stirring at 40 °C for 1.5 h. Subsequently, 2 g of CS was dissolved in 100 mL of 1% (v/v) acetic acid solution with continuous stirring for 30 min to obtain a homogeneous CS solution. Immediately thereafter, 1% (w/w) G was added to the chitosan solution and stirred for an additional 30 min to obtain a cross-linked CS/G solution. Subsequently, 15% (w/w) CNC -S were added, and the resulting mixture was stirred for 3 h. Next, the LEO emulsion was blended into the solution and stirred for an additional hour. The resulting mixture was then deaerated by ultrasonication. Finally, the CS/G/CNC/LEO solution was cast and dried to obtain composite films for subsequent characterization. In addition, the same solution was used for cherry tomato preservation experiments.

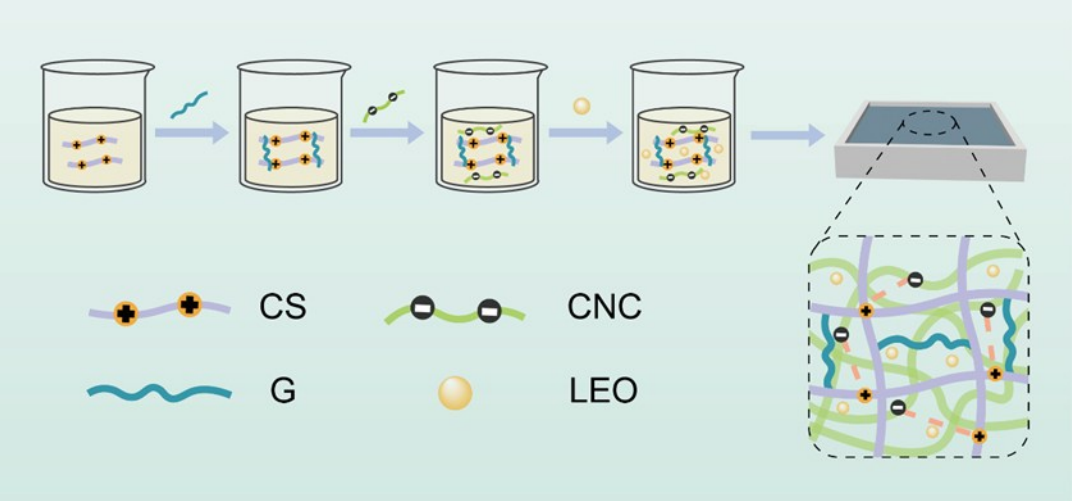

Fig. 1. Preparation process of CS/G/CNC/LEO film

Scanning Electron Microscopy (SEM)

These films were quenched in liquid nitrogen to obtain cross-sections. Then, a layer of gold was sprayed on their surfaces and cross-sections. The images were obtained using a scanning electron microscope (JSM-IT300LV, Japan Electronics Corporation).

Fourier Transform Infrared Spectroscopy

The infrared spectra of the films in the range of 4000 to 500 cm^{-1} were recorded using Shimadzu spectrophotometer (IR Prestige 21). Each analysis recorded 32 scans with a resolution of 4 cm^{-1}.

X-Ray Photoelectron Spectroscopy (XPS)

X-ray photoelectron spectrometer (Thermo Scientific K-Alpha, USA) uses monochromatized Al Kα (hv=1486.6 eV, 12 kV, 6 mA) as the radiation source, with a beam spot of 400 μm. The vacuum degree of the analysis room is better than 5.0×10^{-7} mbar. All spectra were corrected using C 1s at 284.8 eV.

Mechanical Properties

The film sample was cut into a rectangle of 100 mm × 15 mm. A universal material testing machine was used, with an initial distance of 50 mm between the fixtures. The test was conducted at a speed of 100 mm/s.

Thickness was measured using a digital thickness gauge (Model 251, accuracy ± 0.001 mm). At least three replicates were measured for each sample. The average thickness was then employed as a key parameter to assess both mechanical properties and barrier properties of the films.

Water Vapor Permeability

The film was cut into circular specimens with a diameter of 7.8 cm. The water vapor permeability (WVP) of the film was obtained at 23 ℃ and 50% RH using a water vapor transmission rate tester (Guangzhou Xitang). The test unit was measured on an area of 33 cm^2 of the membrane.

Oxygen Permeability

The film was cut into circular specimens with a diameter of 9.6 cm. The oxygen permeability (OP) of the membrane was obtained at 0% RH and 23 °C. The test unit was measured on an area of 50 cm^2 of the membrane, with a sampling interval of 10 seconds.

Water Solubility

The film was soaked in deionized water at 25 ℃ for 24 h and then dried at 105 ℃ until a constant weight was achieved. The water solubility of the membrane was calculated according to Eq. 1,

$$Water\ solubility\ (\%) = \frac{W_1 - W_2}{W_1} \times 100\% \quad (1)$$

where W_1 and W_2 are the weights of the film before and after water immersion, respectively.

Swelling Ratio

The film was immersed in deionized water at room temperature for 24 h. Filter paper was used to absorb the excess moisture, and then the film was weighed. The swelling rate was determined by Eq. 2,

$$Swelling\ ratio\ (\%) = \frac{W_2 - W_1}{W_1} \times 100\% \quad (2)$$

where W_1 is the weight of the dry film sample, and W_2 is the weight of the wet film sample.

Ultraviolet Shielding Property

The ultraviolet transmittance of the film was analyzed using a UV-2700 spectrophotometer (Shimadzu, Japan), using air as a reference. The wavelength range was 200 to 800 nm.

Thermal Property

The thermal properties of the film were analyzed by using a synchronous thermal analyzer (TA, USA). A mass of 5 mg of the film was weighed, and it was heated it in a sealed chamber at a temperature ranging from 40 ° C to 700 ° C with a heating rate of 10 °C/min.

Assessment of Post-Harvest Performance of CS/G/CNC/LEO Film

Uniform, blemish-free cherry tomatoes were purchased locally, rinsed with deionized water, sanitized with 100 mg/L sodium hypochlorite (2 min), and air-dried in a laminar-flow hood. The fruits were randomly allocated to three groups: uncoated control, CS/G/CNC coating, and CS/G/CNC/LEO coating. Each fruit was dip-coated for 30 s, allowed to drain for 2 min, and dried at 25 °C for 2 h to form a continuous film. The samples were stored at (25 ± 1) °C and 60% ± 5% relative humidity for 11 days.

Firmness was determined by equatorial compression (5 mm deformation, 2 mm s^{-1}) using a TA.XTplusC texture analyser (Stable Micro Systems, UK) equipped with a 5 mm cylindrical probe. Total soluble solids (TSS) was measured using a digital pocket refractometer (PAL-1, Atago, Japan). The pH was determined in homogenized juice using a calibrated pH meter (PHS-3C, Lichen, China). Respiration rate was measured using a portable headspace analyzer (MOCON CheckPoint 3, Denmark).

Weight loss was calculated as follows,

$$\text{Weight loss} = (M_0 - M_t)/M_0 \times 100\% \quad (3)$$

where M_0 is the initial mass and M_t is the mass at time t.

Ascorbic acid (V_c) was titrated with standard potassium iodate content (mg/100g) and computed as follows,

$$V_c=(V_k \times V_e \times K_{AA})/(V_s \times m) \times 100 \quad (4)$$

where V_k is the volume of KIO_3 (mL), V_e is the total extract volume (mL), K_{AA} = 0.088 mg/mg, V_s is the aliquot volume (mL), and m is the sample mass (g).

Titratable acidity (TA) was calculated by Eq. 5,

$$TA\ (\%) =(V_{NaOH} \times V_e \times c \times K_c)/(V_s \times m) \times 100\% \quad (5)$$

where V_{NaOH} is the volume consumed by the sodium hydroxide solution (mL); V_e is the total volume of the extract (mL), c is the molar concentration of sodium hydroxide solution (mol/L), K_c is the milliequivalent factor of malic acid (0.067), V_s is the volume of the extract used for titration (mL), and m is the total mass of the pulp.

Statistical Analysis

All measurements were performed in triplicate unless otherwise stated. Data are presented as mean±standard deviation. One-way analysis of variance (ANOVA) was conducted, and significant differences among means were identified by Tukey's HSD test at $p < 0.05$ using SPSS Statistics 27.0.

RESULTS AND DISCUSSION

Morphological Characteristics of the Films

SEM micrographs (Fig. 2) revealed distinct topographical differences among the four formulations. The CS film exhibited a uniform and featureless fracture surface, which confirmed the typical dense but brittle morphology of unmodified chitosan. After genipin treatment, the CS/G film presented a distinct reticular structure, and this structural change reflected the local rearrangement and hardening of the polysaccharide chains formed through cross-linking (Xie *et al*. 2023).

Introducing CNC dramatically altered the morphology: CS/G/CNC films exhibited the highest surface roughness along with well-defined, stratified lamellae in cross-section, which attests to the uniform intercalation and planar orientation of the high-aspect-ratio nanocrystals within the chitosan matrix (Zhang *et al*. 2021).

Incorporation of LEO generated a distinctly different morphology. The CS/G/CNC/LEO surface displayed discrete protuberances and nano- to microscale cavities, which can be attributed to the entrapment and partial volatilization of LEO droplets during drying (Vahedikia *et al*. 2019; Liu *et al*. 2021). Comparable vesicular features have been reported for EO-loaded protein films, where rapid solvent evaporation induces oil-rich domains and local densification of the surrounding polymer (Vahedikia *et al*. 2019). Although isolated voids were visible, the cross-section remained continuous and crack-free, demonstrating that the G/CNC dual network successfully preserved film cohesion despite the presence of hydrophobic inclusions. This observation contrasts with the extensive fracture lines observed in cinnamon-oil/zein systems, reaffirming the structural robustness conferred by the synergistic crosslinking and nanoreinforcement strategy (Talón *et al*. 2017).

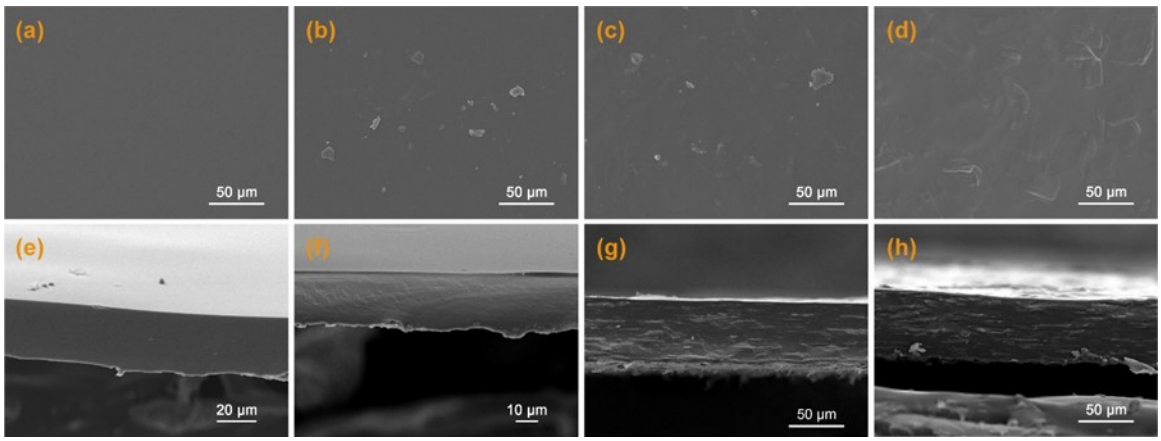

Fig. 2. SEM images of the surface morphology of the sample (a)CS, (b)CS/G, (c)CS/G/CNC, (d) CS/G/CNC/LEO; Cross-sectional SEM images of the sample (e)CS, (f)CS/G, (g)CS/G/CNC, (h) CS/G/CNC/LEO

Interaction Mechanism

FTIR analysis confirmed the stepwise construction of the multicomponent network (Fig. 3). Neat genipin exhibited a broad O–H stretching band at 3200 to 3400 cm^{-1} and a distinct C=O band at 1677 cm^{-1}, along with characteristic epoxy signals at 1205 and 880 cm^{-1}, which are indicative of its ring-opening reaction with primary amines (Teimouri *et al*. 2019).

After cross-linking, all CS-based films retained the characteristic O–H/N–H stretching envelope (3300 to 3400 cm^{-1}) and asymmetric C–H stretching bands (2935/2884 cm^{-1}). However, the amide I band increased in intensity and shifted from 1634 cm^{-1} (CS) to 1631 cm^{-1} (CS/G), providing evidence for the formation of imine (C=N) linkages between G and the amino groups of CS (Zhang *et al*. 2010). In addition, the multiple functional groups present in G can form hydrogen bonds with CS (Liu *et al*. 2019).

In the CS/G/CNC film, the band at 3300 to 3400 cm^{-1} became sharper and more intense than that in the CS/G film, indicating enhanced hydrogen bonding interactions between CS and CNC (Costa *et al*. 2021; Samsalee *et al*. 2026). Furthermore, the amide II band shifted to a lower wavenumber (from 1552 to 1538 cm^{-1}), suggesting strong

electrostatic interactions between the NH_3^+ groups of CS and the SO_3^- groups of CNC, consistent with previous findings (Perumal *et al*. 2018).

The incorporation of LEO resulted in significant broadening and a redshift of the band at 3300 to 3400 cm^{-1}, indicating the formation of additional hydrogen bonds between LEO components and the CS backbone (Cruz-Tirado *et al*. 2020). Concurrently, the intensity of the C–H stretching vibrations (2870 to 2930 cm^{-1}) decreased, suggesting that the fatty chains were entrapped within the dense polymer network. Notably, the absence of aldehyde absorption peaks at 2720 and 2820 cm^{-1} confirmed that no Schiff base reaction occurred between LEO and CS (de Souza *et al*. 2020); therefore, the essential oil was incorporated solely through non-covalent interactions.

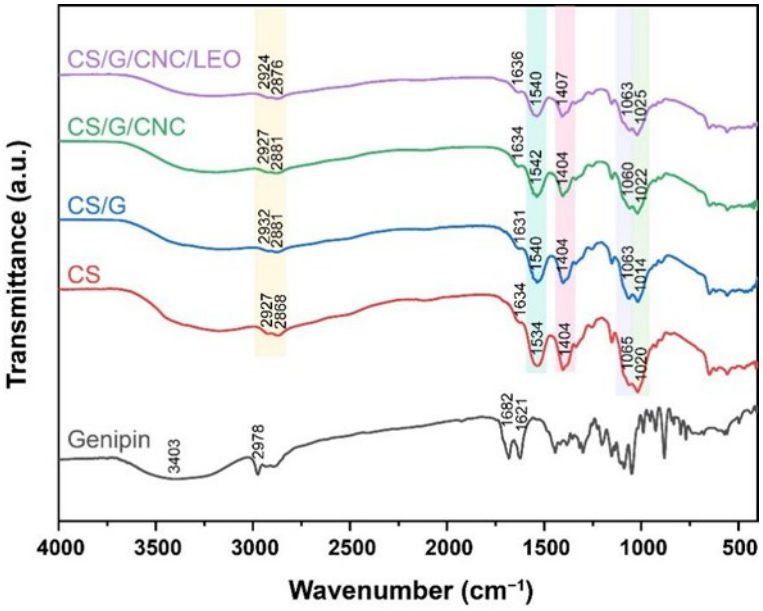

Fig. 3. FTIR spectra of varied films

As shown in Fig. 4, the XPS spectra reveal a marked decrease in the intensity of the characteristic C–O/C–N peak (~286.5 eV) following the sequential addition of G and CNC into the CS matrix. Two principal factors explain this observation. The primary reason is the cross-linking reactions between genipin and the $–NH_2$ groups of CS, which consume C–N bonds and generate C=N linkages. The binding energy of these newly formed C=N bonds overlaps with that of the C–C/C–H region, leading to an apparent attenuation of the original C–O/C–N signal. Consequently, the relative proportion of C–O/C–N bonds decreases (Liu *et al*. 2013). Secondly, the abundant hydroxyl groups (–OH) on the surface of CNC form an extensive hydrogen-bonding network with C–O/C–N functional groups (*e.g*., primary and secondary hydroxyls and residual acetyl groups) in the chitosan chains (Chen *et al*. 2019). These strong interfacial interactions may induce local electron density redistribution and partially suppress photoelectron emission from C–O/C–N bonds. Collectively, these spectral changes confirm genipin-mediated cross-linking and the establishment of robust interfacial interactions between CS and CNC.

The mechanistic sequence proposed by Butler *et al*. (2003) supports these observations. An initial nucleophilic attack by the $–NH_2$ groups of chitosan at the C-3 position of genipin triggers dihydropyran ring opening, forming tertiary amine adducts. Subsequently, a slower substitution at the ester carbonyl yields amide linkages, collectively

producing a bifunctional and highly stable network with significantly lower cytotoxicity than glutaraldehyde-derived cross-links (Mi *et al*. 2005). Further oxidative self-polymerization of genipin introduces additional cross-linking, accompanied by the emergence of a characteristic deep-blue coloration (Tripathi *et al*. 2024).

In summary, the combined FTIR and XPS results demonstrate that G forms covalent C=N and amide cross-links, CNCs reinforce the matrix through strong hydrogen bonding and electrostatic interactions, and LEO is physically immobilized within the hybrid network, resulting in a cohesive and multifunctional film architecture.

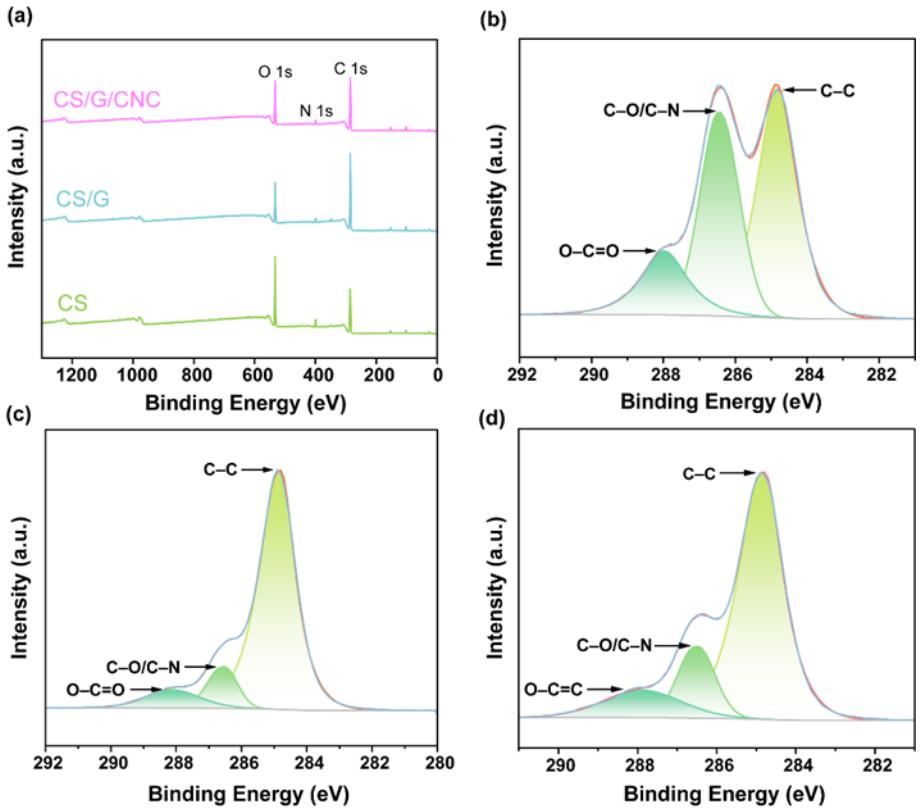

Fig. 4. XPS spectra of CS, CS/G, and CS/G/CNC. (a) the total spectrum of CS, CS/G, and CS/G/CNC; (b) the C1s spectrum of CS; (c) the O1s spectrum of CS/G; (d) the N1s spectrum of CS/G/CNC

Mechanical Properties

The tensile property of the films (Fig. 5) provides clear evidence of the structural changes caused by each additive. The tensile strength (TS) of the pure CS film was 27.22 ± 2.06 MPa, while its elongation at break (EB) did not exceed 1%.

Genipin cross-linking increased TS to 32.49 ± 3.26 MPa, which is about a 19% increase, but reduced EB to 0.54 ± 0.1%. This stiffer behavior is due to the formation of covalent C=N and amide bonds that connect adjacent polymer chains and create a denser and less flexible network (Lopes *et al*. 2023). The addition of 15wt% CNC further increased TS to 58 to 60 MPa, which is about 2.2 times higher than that of pure CS. This result indicates effective stress transfer from the CS matrix to the rigid nanocrystals. These findings support the proposed mechanism in which CNC acts as a physical cross-linking agent and works together with genipin cross-linking (De France *et al*. 2021).

The addition of the LEO nano-emulsion led to a slight decrease in TS to approximately 50 MPa, accompanied by a marked increase in elongation at break to approximately 10%. The presence of oil droplets and surfactant molecules between polymer chains weakens intermolecular interactions, increases free volume, and improves chain mobility, which are typical features of a plasticizing effect (Norcino *et al*. 2020). Although the overall strength decreased, the final tensile strength remained over 80% higher than that of pure CS. At the same time, the improved flexibility is beneficial for handling and sealing performance.

Overall, these results show that a balance between strength and flexibility can be achieved by adjusting the amounts of cross-linking agent, reinforcing filler, and plasticizing essential oil. This allows the design of films suitable for different packaging applications.

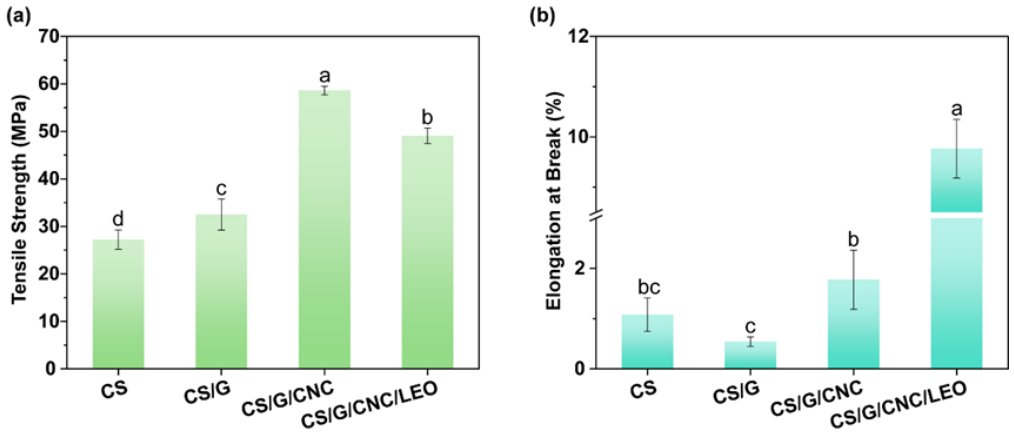

Fig. 5. (a) Tensile strength and (b) elongation at break

Swelling and Solubility

Resistance to aqueous environments is a critical criterion for films used in high-moisture food applications. Two complementary parameters were evaluated. The swelling ratio reflects the extent of water uptake and polymer relaxation, while water solubility represents the mass loss caused by the leaching of low-molecular-weight or weakly bound components (Ulfah *et al*. 2018).

The combined modification with G and CNC significantly improved water resistance. Both the swelling ratio and solubility of the CS/G/CNC film decreased compared with pure CS (Fig. 6). These reductions can be attributed to the formation of a denser hydrogen-bonded and covalently cross-linked network. This network restricts the mobility of hydrophilic hydroxyl and amino groups, reduces free volume, and limits solvent penetration (Zhu *et al*. 2024). The incorporation of LEO further reduced swelling, with a 62% decrease relative to CS/G/CNC, while slightly increasing the overall solubility. This result can be explained by two effects. LEO domains block water diffusion pathways and reduce matrix swelling. At the same time, the presence of oil droplets and surfactants disrupts polymer interactions and creates loosely bound regions that are more prone to leaching, which increases the measured solubility (Rhim *et al*., 2000). A similar trend, in which swelling decreases while solubility increases, has been reported for gelatin and chitosan films containing thyme and clove essential oils (Gómez-Estaca *et al*. 2010). This behavior reflects the complex influence of hydrophobic additives on film and water interactions.

Overall, the CS/G/CNC/LEO film showed minimal dimensional change during water exposure and maintains acceptable, although slightly higher solubility. This indicates a balance between water resistance for packaging performance and controlled degradability for environmental considerations.

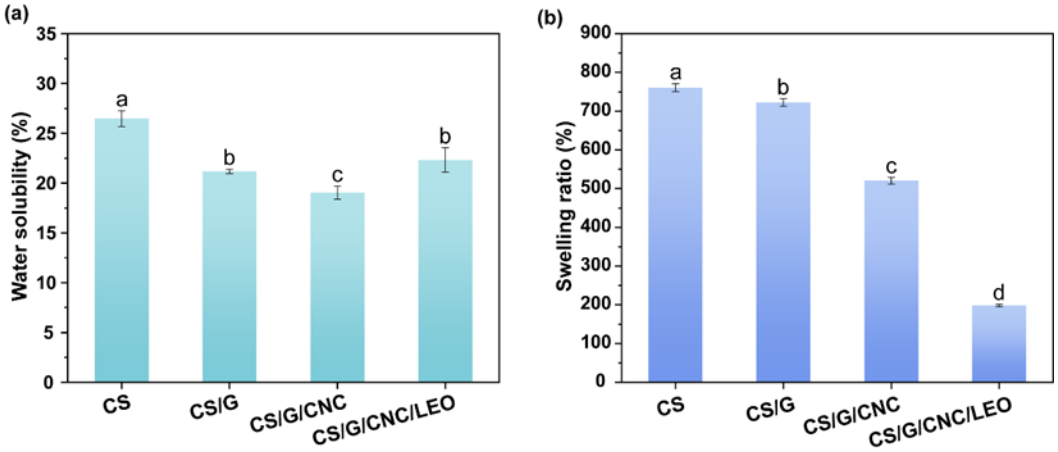

Fig. 6. (a) Water solubility of films with different compositions and (b) swelling ratio

Barrier Property Analysis of Films

Effective food packaging must simultaneously limit moisture transfer and oxygen entry, as these are two main causes of microbial growth and oxidative spoilage (Alizadeh Sani *et al*. 2025).

The densely cross-linked CS/G film showed the lowest WVP among all samples, confirming that G cross-linking reduces free volume and limits sites for water absorption (Xie *et al*. 2023). Adding CNC alone slightly increased WVP to 7.6×10^{-12} g·cm/(cm^2·s·Pa), because the hydrophilic surface of the nanofiller can absorb water and create additional micro-diffusion pathways (Sultan *et al*. 2023). Notably, the subsequent addition of LEO reduced WVP to 6.5×10^{-12} g·cm/(cm^2·s·Pa), which is close to that of pure CS. This improvement is attributed to the hydrophobic nature of the citral-rich oil and the increased tortuosity caused by well-dispersed oil droplets, which force water molecules to follow longer and more complex paths (Almasi *et al*. 2020). Overall, this leads to a reduction in the film's hydrophilicity, even in the presence of CNC.

Polysaccharide films are intrinsically good oxygen barriers due to their highly organized hydrogen-bonded networks (Marand *et al*. 2023). The CS/G/CNC film exhibited the lowest OP among all formulations, which can be attributed to genipin-induced compaction that reduces free volume, along with uniform CNC dispersion that fills interstitial voids and increases crystallinity. These factors collectively lengthen the diffusion pathway for small gas molecules (Vilarinho *et al*. 2018; Criado *et al*. 2020).

The introduction of LEO caused a moderate increase in OP compared with CS/G/CNC, which is attributed to a plasticizing effect. LEO and its carrier surfactant disrupt tight chain packing, increase segmental mobility, and facilitate gas diffusion (Wongphan *et al*. 2023). Even so, the CS/G/CNC/LEO film maintained an oxygen barrier superior to that of pure CS while providing the best WVP performance among the reinforced systems. This offers a favorable balance for applications such as fresh-produce packaging, where both moisture resistance and controlled O_2 transmission are required.

Table 1. Thickness, Water Vapor Permeability, and Oxygen Permeability of Different Films

Samples	Thickness (mm)	WVP ($\times10^{-12}$g·cm/cm^2·s·Pa)	OP ($\times10^{-16}$cm^3/cm^2·s·Pa)
CS	0.055 ± 0.004^d	7.31 ± 0.99^a	6.69 ± 0.21^a
CS/G	0.067 ± 0.004^c	5.05 ± 0.51^c	3.84 ± 0.14^c
CS/G/CNC	0.084 ± 0.002^b	7.60 ± 0.29^a	3.61 ± 0.08^c
CS/G/CNC/LEO	0.091 ± 0.002^a	54.93 ± 0.58^b	4.71 ± 0.21^b

Optical Performance

Ultraviolet exposure is an important abiotic factor that causes pigment loss, nutrient degradation, and softening in fresh produce (Chen *et al*. 2024). Therefore, effective ultraviolet blocking is a desirable property for active packaging materials.

Among the four formulations, the CS/G/CNC film showed the strongest ultraviolet barrier. The transmittance at 280 nm decreased by about 95%, and the overall film opacity increased by 38% compared with pure CS (Fig. 7a). This improvement can be explained by two optical effects. One is selective absorption by conjugated chromophores formed during G cross-linking (Lin *et al*. 2020). The other is multiple scattering caused by well-dispersed CNCs. The difference in refractive index between CNCs and the chitosan matrix increases the light path length and enhances light attenuation (Criado *et al*. 2020).

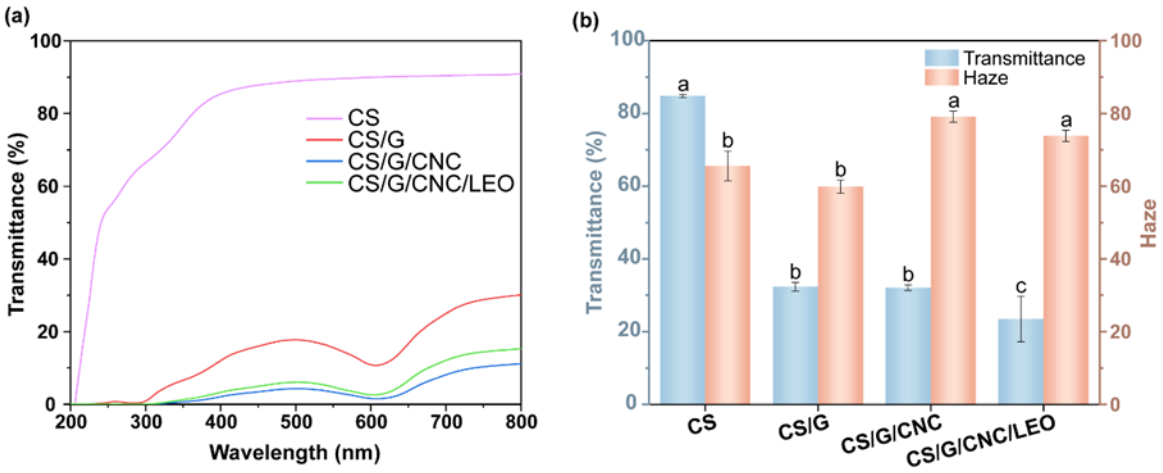

Fig. 7. The film with different compositions (a) Ultraviolet spectra (b) transmittance and haze

Pure CS was nearly colorless and showed high transparency, with transmittance greater than 85% at 600 nm and low haze. This property is not suitable for products that are sensitive to ultraviolet light. All composite films appeared darker and more turbid due to chromophore formation and the addition of fillers. The presence of CNC further increased haze, which is consistent with higher surface roughness and reduced free volume that promote diffuse reflection (Yadav *et al*. 2021).

The addition of LEO caused a further decrease in visible light transmittance. This effect is related to increased scattering and partial aggregation of small oil droplets within

the polymer matrix (Atarés and Chiralt 2016). Although the CS/G/CNC/LEO film showed slightly lower ultraviolet blocking than CS/G/CNC, likely due to increased free volume caused by plasticization, it still blocked more than 90% of radiation below 320 nm. This indicates that the film provides sufficient protection for light-sensitive foods while also offering antimicrobial properties.

Thermal Property

The thermal decomposition profiles of the films showed several distinct stages typical of chitosan-based systems (Fig. 8). The initial mass loss observed between 40 and 103 °C corresponds to the removal of physically absorbed moisture and residual acetic acid. A second degradation stage, occurring between 103 and 230 °C, is attributed to the evaporation or decomposition of low-molecular-weight components such as glycerol. The main degradation stage, from 230 to 400 °C, involves extensive depolymerization of chitosan and cleavage of glycosidic bonds, resulting in an approximate mass loss of 30%, which is consistent with previous reports (Riaz *et al*. 2020).

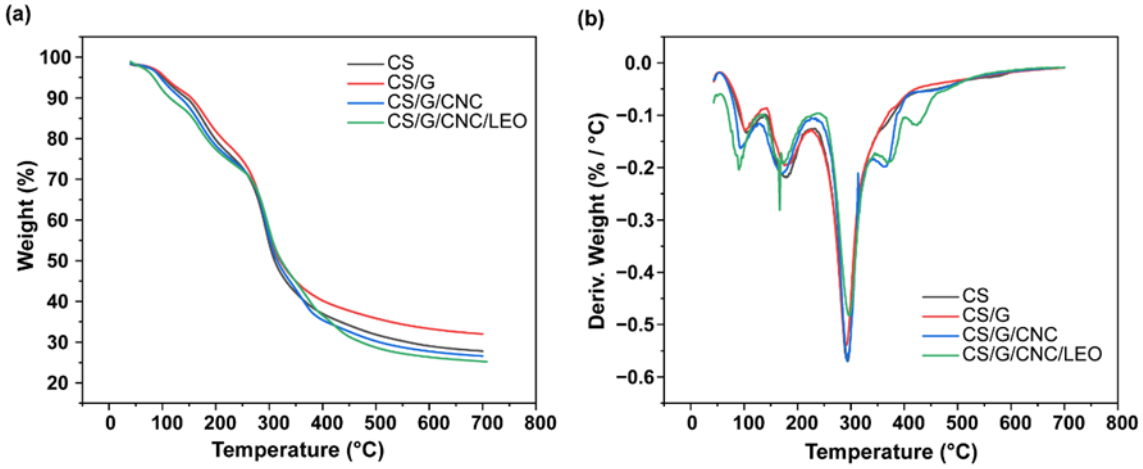

Fig. 8. (a) TG curves and (b) DTG curves of films with different components

The incorporation of CNC introduced a distinct shoulder or secondary DTG peak between 330 and 400 °C, suggesting effective integration of the nanocrystals into the polymer matrix and reflecting their inherent thermal decomposition behavior (Corsello et al. 2017). Both CS/G and CS/G/CNC films exhibited continuous mass loss between 100 and 270 °C, with total losses of 25.8% and 30.8%, respectively, slightly exceeding that of neat CS. This behavior may be attributed to the reduced thermal stability of the partially deacetylated chitosan backbone following genipin cross-linking, which introduces rigid yet thermally sensitive structures (Tavares *et al.* 2020).

The CS/G/CNC/LEO composite demonstrated enhanced thermal stability above 280 °C, as evidenced by a delayed onset of major decomposition compared to the other films. Additionally, a minor weight loss was observed between 400 and 460 °C, which may be associated with the degradation of LEO-derived components or thermally resistant composite domains (Chen *et al.* 2023). Despite this improvement at elevated temperatures, the total mass loss of the CS/G/CNC/LEO system exceeded that of films without LEO. This effect can be attributed to the essential oil modifying intermolecular interactions and introducing thermally labile components into the network (Zhang *et al.* 2019).

Overall, these results indicate that CNC reinforcement and genipin cross-linking alter the thermal decomposition behavior, while the incorporation of LEO influences both thermal stability and the multi-step degradation pattern of the resulting biocomposite.

The Preservation Performance of CS/G/CNC/LEO Film

An 11-day room-temperature study was conducted to evaluate the visual quality of cherry tomatoes coated with the CS/G/CNC/LEO composite. During the first five days, the coated samples showed no visible changes in surface appearance, while the control samples already showed slight wrinkling (Fig. 9). By day 11, the control samples showed severe shrinkage and surface collapse, which are typical signs of significant water loss. In contrast, the CS/G/CNC/LEO-coated tomatoes maintained their firmness, smooth surface, and bright color, with no visible mold formation. The composite coating, therefore, effectively delayed visible deterioration compared with both the control and the CS/G/CNC reference film.

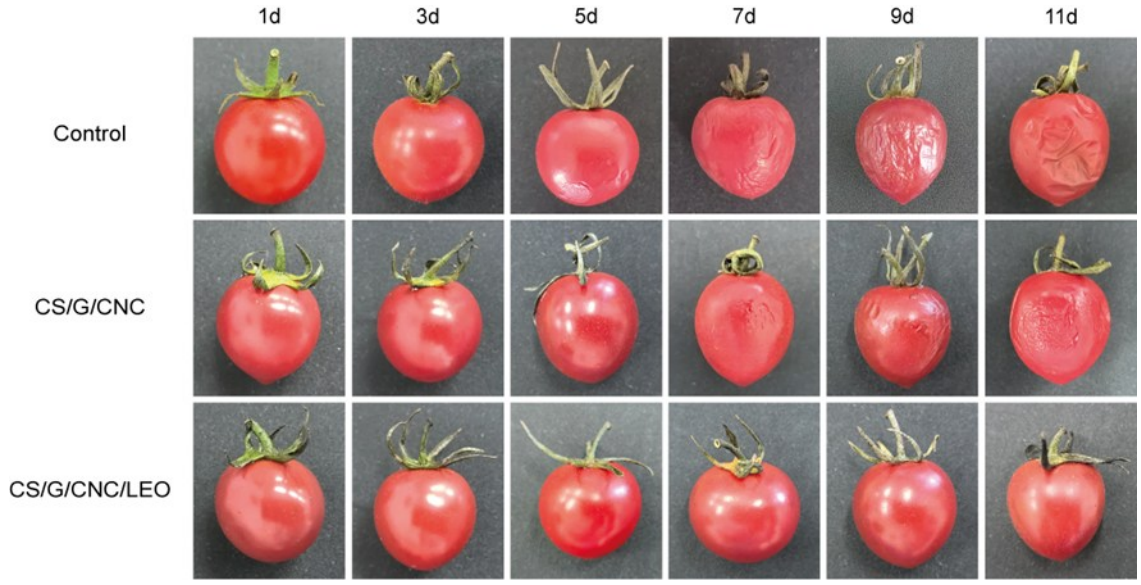

Fig. 9. Physical appearance of tomato during storage at room temperature

Figure 10(a) shows a continuous increase in weight loss for all groups, with the fastest increase observed in the control. After 11 days, fruit coated with CS/G/CNC/LEO showed only 9.04% weight loss, which was lower than the 12.21% observed in the control and lower than the value for the CS/G/CNC film. This reduction can be attributed to the formation of a stable moisture barrier that reduces transpiration and water loss during respiration (Flores-López *et al*. 2016). The improved performance of the LEO-containing film is related to its more compact structure, formed by the presence of essential oil, which further limits water vapor diffusion.

Changes in firmness followed a similar trend (Fig. 10(b)). The control fruit lost 41.8% of its initial firmness, while CS/G/CNC and CS/G/CNC/LEO treatments limited the decrease to 37.8% and 31.5%, respectively. This improved texture retention is related to reduced breakdown of cell wall components and lower water loss, as the coatings help control gas and moisture exchange (Hu *et al*., 2011).

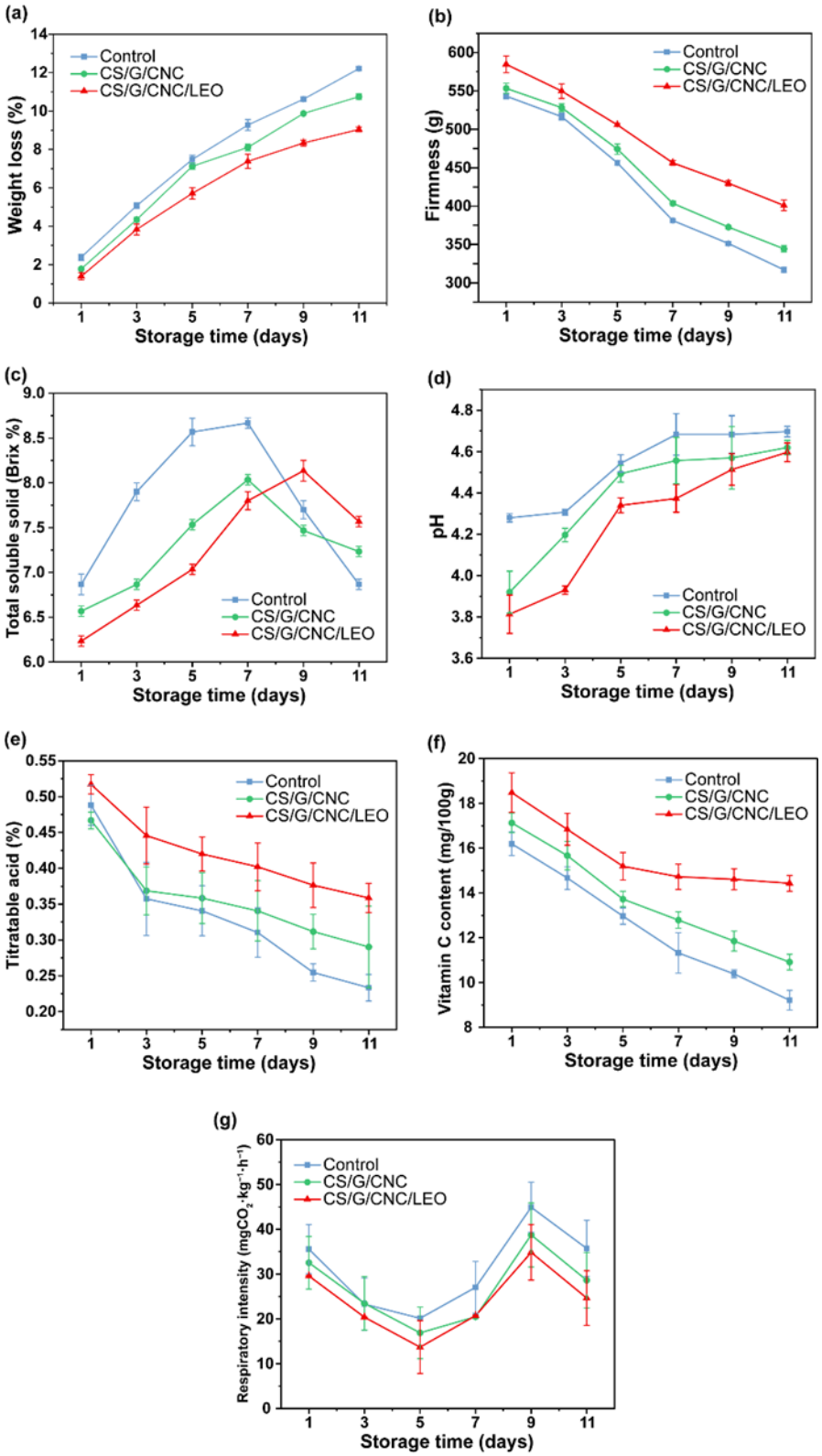

Fig. 10. Influence of different storage configurations on (a) weight loss, (b) firmness, (c) total soluble solids, (d) pH, (e) titratable acid, (f) vitamin C content, and (g) respiratory intensity

All samples showed an initial increase in total soluble solids, followed by a gradual decrease during storage (Fig. 10(c)). The CS/G/CNC/LEO group maintained the highest values throughout the storage period, indicating better retention of sugars and organic acids and improved flavor quality.

A gradual increase in pH was observed in all groups (Fig. 10(d)), which is related to the consumption of organic acids during metabolism. The CS/G/CNC/LEO coating consistently showed the lowest pH values, indicating that it slowed acid loss and delayed ripening (Al-Dairi *et al*. 2021).

TA decreased in all treatments (Fig. 10(e)). By day 11, fruit coated with CS/G/CNC/LEO retained 0.36% total acidity, corresponding to a 30.66% loss. This performance was better than that of CS/G/CNC with 0.29 % and a 37.81% loss, and the control with 0.23% and a 52.17% loss. These results indicate that the composite film slows the breakdown of organic acids and helps maintain sensory quality.

Vitamin C content decreased over time (Fig. 10(f)). However, the CS/G/CNC/LEO film limited the reduction to 21.9%, which is about half of the 43.1% loss observed in the control. This improved retention is related to reduced oxygen entry and lower oxidative damage within the coated fruit (Wu *et al*. 2016).

Respiration profiles (Fig. 10(g)) showed a peak around day 9 for all groups. The CS/G/CNC/LEO treatment reduced the overall respiration intensity and maintained the lowest CO_2 production at day 11, indicating effective control of gas exchange and delayed aging.

In summary, the CS/G/CNC/LEO coating provided the best preservation performance, outperforming both the uncoated control and the CS/G/CNC film across all measured indicators. These results highlight the potential of the CS/G/CNC/LEO system as an alternative to traditional petroleum-based packaging for high-value fresh produce.

Limitations and Future Work

Although this study showed the potential application of the CS/G/CNC/LEO film as an active packaging material, several limitations remain. First, the film is made from bio-based materials and may be edible, but its safety has not been fully evaluated. Second, future studies should examine large-scale production, the release behavior of active components, and preservation performance for a wider range of fruits. Third, the leaching experiments to assess film stability were not conducted. Fourth, although chitosan is biodegradable, the crosslinking process used in this study may reduce its degradation in the environment by forming non-natural bonds and limiting enzyme access. These issues need further study.

CONCLUSIONS

1. This study developed a multifunctional chitosan film composed entirely of biobased components. Genipin provided covalent cross-linking, sulfonated cellulose nanocrystals provided structural reinforcement, and lemongrass essential oil provided antibacterial activity. Comprehensive physical and chemical analyses confirmed the formation of a dense and well-connected network through combined covalent interactions (C=N or amide) and non-covalent interactions (hydrogen bonding or electrostatic attraction). As a result, the tensile strength of the CS/G/CNC/LEO film increased by more than 80%, while water vapor and oxygen permeability decreased

significantly. The swelling ratio decreased by 74%, and the film showed strong ultraviolet blocking ability.

2. When used as a coating for cherry tomatoes, the composite reduced weight loss to less than 10%, maintained firmness, reduced respiration intensity, and slowed the decrease in total soluble solids, titratable acid, and vitamin C content. As a result, the shelf life was extended by at least six days compared with uncoated fruit.
3. Although the developed materials exhibit considerable potential, their toxicological safety has not yet been systematically assessed. To address this research gap, the present study provides critical data to support the development of safer food packaging materials.

ACKNOWLEDGMENTS

The authors are thankful for the support from Science Project of Tianjin Municipal Science and Technology Bureau (Grant number: 22YDTPJC00860).

REFERENCES CITED

Adukwu, E. C., Bowles, M., Edwards-Jones, V., and Bone, H. (2016). "Antimicrobial activity, cytotoxicity and chemical analysis of lemongrass essential oil (*Cymbopogon flexuosus*) and pure citral," *Appl. Microbiol. Biotechnol.* 100(22), 9619-9627. https://doi.org/10.1007/s00253-016-7807-y

Ahmad, U., Ishaq, A., and Khalid, N. (2026). "Carboxymethyl cellulose-based edible coatings emulsified with lemongrass oil for enhancing the storage stability of refrigerated broiler meat," *Food Sci. Anim. Resour*. 46(1), 7. https://doi.org/10.1007/s44463-025-00045-6

Ahmed, R., ul ain Hira, N., Wang, M., Iqbal, S., Yi, J., and Hemar, Y. (2024). "Genipin, a natural blue colorant precursor: Source, extraction, properties, and applications," *Food Chem.* 434, article 137498. https://doi.org/10.1016/j.foodchem.2023.137498

Akhtar, M., and Ding, R. (2017). "Covalently cross-linked proteins & polysaccharides: Formation, characterisation and potential applications," *Curr. Opin. Colloid Interface Sci.* 28, 31-36. https://doi.org/10.1016/j.cocis.2017.01.002

de Albuquerque Sousa, T. C., Rosas, A. L. G., Rombaldi, C. V., Gandra, E. Á., and Meinhart, A. D. (2026). "Lemongrass essential oil incorporated into oat starch cryogel contributes to the preservation of strawberries stored under refrigeration," *Food Bioprocess Technol*. 19(2), article 94. https://doi.org/10.1007/s11947-025-04167-z

Al-Dairi, M., Pathare, P. B., and Al-Yahyai, R. (2021). "Chemical and nutritional quality changes of tomato during postharvest transportation and storage," *J. Saudi Soc. Agric. Sci.* 20(6), 401-408. https://doi.org/10.1016/j.jssas.2021.05.001

Alizadeh Sani, M., Khezerlou, A., Rezvani-Ghalhari, M., McClements, D. J., and Varma, R. S. (2025). "Advanced carbon-based nanomaterials: Application in the development of multifunctional next-generation food packaging materials," *Adv. Colloid Interface Sci.* 339, article 103422. https://doi.org/10.1016/j.cis.2025.103422

Almasi, H., Azizi, S., and Amjadi, S. (2020). "Development and characterization of

pectin films activated by nanoemulsion and pickering emulsion stabilized marjoram (*Origanum majorana* L.) essential oil," *Food Hydrocoll.* 99, article 105338. https://doi.org/10.1016/j.foodhyd.2019.105338

Atarés, L., and Chiralt, A. (2016). "Essential oils as additives in biodegradable films and coatings for active food packaging," *Trends Food Sci. Technol.* 48, 51-62. https://doi.org/10.1016/j.tifs.2015.12.001

Babaei-Ghazvini, A., Acharya, B., and Korber, D. R. (2022). "Multilayer photonic films based on interlocked chiral-nematic cellulose nanocrystals in starch/chitosan," *Carbohydr. Polym.* 275, article 118709. https://doi.org/10.1016/j.carbpol.2021.118709

Butler, M. F., Ng, Y., and Pudney, P. D. A. (2003). "Mechanism and kinetics of the crosslinking reaction between biopolymers containing primary amine groups and genipin," *J. Polym. Sci. Part A: Polym. Chem.* 41(24), 3941-3953. https://doi.org/10.1002/pola.10960

Chen, K., Tian, R., Jiang, J., Xiao, M., Wu, K., Kuang, Y., Deng, P., Zhao, X., and Jiang, F. (2024). "Moisture loss inhibition with biopolymer films for preservation of fruits and vegetables: A review," *Int. J. Biol. Macromol.* 263, article 130337. https://doi.org/10.1016/j.ijbiomac.2024.130337

Chen, L., McClements, D. J., Cheng, H., Qiu, C., Long, J., Ji, H., Meng, M., and Jin, Z. (2023). "Structure and properties of flexible starch-based double network composite films induced by dopamine self-polymerization," *Carbohydr. Polym.* 299, article 120106. https://doi.org/10.1016/j.carbpol.2022.120106

Chen, Q.-J., Zhou, L.-L., Zou, J.-Q., and Gao, X. (2019). "The preparation and characterization of nanocomposite film reinforced by modified cellulose nanocrystals," *Int. J. Biol. Macromol.* 132, 1155-1162. https://doi.org/10.1016/j.ijbiomac.2019.04.063

Corsello, F. A., Bolla, P. A., Anbinder, P. S., Serradell, M. A., Amalvy, J. I., and Peruzzo, P. J. (2017). "Morphology and properties of neutralized chitosan-cellulose nanocrystals biocomposite films," *Carbohydr. Polym.* 156, 452-459. https://doi.org/10.1016/j.carbpol.2016.09.031

Costa, S. M., Ferreira, D. P., Teixeira, P., Ballesteros, L. F., Teixeira, J. A., and Fangueiro, R. (2021). "Active natural-based films for food packaging applications: The combined effect of chitosan and nanocellulose," *Int. J. Biol. Macromol.* 177, 241-251. https://doi.org/10.1016/j.ijbiomac.2021.02.105

Criado, P., Fraschini, C., Salmieri, S., and Lacroix, M. (2020). "Cellulose nanocrystals (CNCs) loaded alginate films against lipid oxidation of chicken breast," *Food Res. Int*. 132, article 109110. https://doi.org/10.1016/j.foodres.2020.109110

Cruz-Tirado, J. P., Barros Ferreira, R. S., Lizárraga, E., Tapia-Blácido, D. R., Silva, N. C. C., Angelats-Silva, L., and Siche, R. (2020). "Bioactive andean sweet potato starch-based foam incorporated with oregano or thyme essential oil," *Food Packag. Shelf Life* 23, article 100457. https://doi.org/10.1016/j.fpsl.2019.100457

De France, K., Zeng, Z., Wu, T., and Nyström, G. (2021). "Functional materials from nanocellulose: Utilizing structure-property relationships in bottom-up fabrication," *Adv. Mater.* 33(28), article 2000657. https://doi.org/10.1002/adma.202000657

Deng, H., Lin, P., Xin, S., Huang, R., Li, W., Du, Y., Zhou, X., and Yang, J. (2012). "Quaternized chitosan-layered silicate intercalated composites based nanofibrous mats and their antibacterial activity," *Carbohydr. Polym.* 89(2), 307-313. https://doi.org/10.1016/j.carbpol.2012.02.009

Doustdar, F., Olad, A., and Ghorbani, M. (2022). "Effect of glutaraldehyde and calcium chloride as different crosslinking agents on the characteristics of chitosan/cellulose nanocrystals scaffold," *Int. J. Biol. Macromol.* 208, 912-924. https://doi.org/10.1016/j.ijbiomac.2022.03.193

Flores-López, M. L., Romaní, A., Cerqueira, M. A., Rodríguez-García, R., Jasso de Rodríguez, D., and Vicente, A. A. (2016). "Compositional features and bioactive properties of whole fraction from aloe vera processing," *Ind. Crops Prod.* 91, 179-185. https://doi.org/10.1016/j.indcrop.2016.07.011

Gan, P. G., Sam, S. T., Abdullah, M. F., Omar, M. F., and Tan, W. K. (2021). "Water resistance and biodegradation properties of conventionally-heated and microwave-cured cross-linked cellulose nanocrystal/chitosan composite films," *Polym. Degrad. Stab.* 188, article 109563. https://doi.org/10.1016/j.polymdegradstab.2021.109563

Gómez-Estaca, J., López De Lacey, A., López-Caballero, M. E., Gómez-Guillén, M. C., and Montero, P. (2010). "Biodegradable gelatin-chitosan films incorporated with essential oils as antimicrobial agents for fish preservation," *Food Microbiol.* 27(7), 889-896. https://doi.org/10.1016/j.fm.2010.05.012

Hu, Q., Fang, Y., Yang, Y., Ma, N., and Zhao, L. (2011). "Effect of nanocomposite-based packaging on postharvest quality of ethylene-treated kiwifruit (*Actinidia deliciosa*) during cold storage," *Food Res. Int.* 44(6), 1589-1596. https://doi.org/10.1016/j.foodres.2011.04.018

Huang, W., Xu, H., Xue, Y., Huang, R., Deng, H., and Pan, S. (2012). "Layer-by-layer immobilization of lysozyme-chitosan-organic rectorite composites on electrospun nanofibrous mats for pork preservation," *Food Res. Int.* 48(2), 784-791. https://doi.org/10.1016/j.foodres.2012.06.026

Kaewklin, P., Siripatrawan, U., Suwanagul, A., and Lee, Y. S. (2018). "Active packaging from chitosan-titanium dioxide nanocomposite film for prolonging storage life of tomato fruit," *Int. J. Biol. Macromol.*112, 523-529. https://doi.org/10.1016/j.ijbiomac.2018.01.124

Kalita, P., Pathak, M. P., Barbhuiya, P. A., and Nongkhlaw, F. T. (2025). "Natural sulfated polysaccharides as biomacromolecule in management of metabolic disorders: A comprehensive review," *Int. J. Biol. Macromol.* 317, article 144856. https://10.1016/j.ijbiomac.2025.144856

Khan, A., Salmieri, S., Fraschini, C., Bouchard, J., Riedl, B., and Lacroix, M. (2014). "Genipin cross-linked nanocomposite films for the immobilization of antimicrobial agent," *ACS Appl. Mater. Interfaces,* 6(17), 15232-15242. https://doi.org/10.1021/am503564m

Ko, M., Jang, T., Yoon, S., Lee, J., Choi, J.-H., Choi, J.-W., and Park, J.-A. (2024). "Synthesis of recyclable and light-weight graphene oxide/chitosan/genipin sponges for the adsorption of diclofenac, triclosan, and microplastics," *Chemosphere*, 356, article 141956. https://doi.org/10.1016/j.chemosphere.2024.141956

Lin, H.-C., Wang, B.-J., and Weng, Y.-M. (2020). "Development and characterization of sodium caseinate edible films cross-linked with genipin," *LWT* 118, article 108813. https://doi.org/10.1016/j.lwt.2019.108813

Liu, D.-K., Xu, C.-C., Guo, C.-X., and Zhang, X.-X. (2020). "Sub-zero temperature preservation of fruits and vegetables: A review," *J. Food Eng*. 275, article 109881. https://doi.org/10.1016/j.jfoodeng.2019.109881

Liu, H., Li, J., Ren, N., Qiu, J., and Mou, X. (2013). "Graphene oxide-reinforced biodegradable genipin-cross-linked chitosan fluorescent biocomposite film and its

cytocompatibility," *Int. J. Nanomedicine* 2013, article 3415. https://doi.org/10.2147/IJN.S51203

Liu, Y., Cai, Z., Sheng, L., Ma, M., Xu, Q., and Jin, Y. (2019). "Structure-property of crosslinked chitosan/silica composite films modified by genipin and glutaraldehyde under alkaline conditions," *Carbohydr. Polym.* 215, 348-357. https://doi.org/10.1016/j.carbpol.2019.04.001

Liu, Z., Lin, D., Shen, R., Zhang, R., Liu, L., and Yang, X. (2021). "Konjac glucomannan-based edible films loaded with thyme essential oil: Physical properties and antioxidant-antibacterial activities," *Food Packag. Shelf Life* 29, article 100700. https://doi.org/10.1016/j.fpsl.2021.100700

Lopes, J., Ferreira, P., Coimbra, M. A., and Gonçalves, I. (2023). "Influence of glycerol, eggshells, and genipin on hydrophobicity and rigidity of antioxidant locust bean milling dust-derived bioplastics," *LWT* 188, article 115409. https://doi.org/10.1016/j.lwt.2023.115409

Marand, S. A., Almasi, H., Amjadi, S., Alamdari, N. G., and Salmasi, S. (2023). "*Ixiolirion tataricum* mucilage/chitosan based antioxidant films activated by free and nanoliposomal fennel essential oil," *Int. J. Biol. Macromol.* 230, article 123119. https://doi.org/10.1016/j.ijbiomac.2022.123119

Mi, F., Shyu, S., and Peng, C. (2005). "Characterization of ring-opening polymerization of genipin and pH-dependent cross-linking reactions between chitosan and genipin," *J. Polym. Sci. Part A: Polym. Chem.* 43(10), 1985-2000. https://doi.org/10.1002/pola.20669

Mohd Daud, I. S., Mahmud Ab Rashid, N. K., Palmer, J., and Flint, S. (2026). "From extraction to application: nanoemulsified lemongrass oil for biofilm and spore control in food preservation," *Int. J. Biol. Macromol*. 450, article 111654. https://doi.org/10.1016/j.ijfoodmicro.2026.111654

Mourão, P. A. S., and Pereira, M. S. (1999). "Searching for alternatives to heparin: sulfated fucans from marine invertebrates," *Trends Cardiovasc. Med.* 9(8), 225-232. https://doi.org/10.1016/S1050-1738(00)00032-3

Norcino, L. B., Mendes, J. F., Natarelli, C. V. L., Manrich, A., Oliveira, J. E., and Mattoso, L. H. C. (2020). "Pectin films loaded with copaiba oil nanoemulsions for potential use as bio-based active packaging," *Food Hydrocoll.* 106, article 105862. https://doi.org/10.1016/j.foodhyd.2020.105862

Pereira, M. B. B., França, D. B., Araújo, R. C., Silva Filho, E. C., Rigaud, B., Fonseca, M. G., and Jaber, M. (2020). "Amino hydroxyapatite/chitosan hybrids reticulated with glutaraldehyde at different pH values and their use for diclofenac removal," *Carbohydr. Polym.* 236, article 116036. https://doi.org/10.1016/j.carbpol.2020.116036

Perumal, A. B., Sellamuthu, P. S., Nambiar, R. B., and Sadiku, E. R. (2018). "Development of polyvinyl alcohol/chitosan bio-nanocomposite films reinforced with cellulose nanocrystals isolated from rice straw," *Appl. Surf. Sci. 4th International Conference on Nanoscience and Nanotechnology* 449, 591-602. https://doi.org/10.1016/j.apsusc.2018.01.022

Poznanski, P., Hameed, A., and Orczyk, W. (2023). "Chitosan and chitosan nanoparticles: Parameters enhancing antifungal activity," *Molecules* 28(7), article 2996. https://doi.org/10.3390/molecules28072996

Rabbani, A., Khaliq, A., Mudgil, P., Maqsood, S., and Nazir, A. (2026). "Recent advances in lemongrass essential oil: food safety, preservation, and bioactivity in food systems," *Compr. Rev. Food Sci. Food Saf*. 25(1), article e70350.

https://doi.org/10.1111/1541-4337.70350

Reesha, K. V., Panda, S. K., Bindu, J., and Varghese, T. O. (2015). "Development and characterization of an LDPE/chitosan composite antimicrobial film for chilled fish storage," *Int. J. Biol. Macromol.* 79, 934-942. https://doi.org/10.1016/j.ijbiomac.2015.06.016

Rhim, J. W., Gennadios, A., Handa, A., Weller, C. L., and Hanna, M. A. (2000). "Solubility, tensile, and color properties of modified soy protein isolate films," *J. Agric. Food Chem.* 48(10), 4937-4941. https://doi.org/10.1021/jf0005418

Riaz, A., Lagnika, C., Luo, H., Dai, Z., Nie, M., Hashim, M. M., Liu, C., Song, J., and Li, D. (2020). "Chitosan-based biodegradable active food packaging film containing Chinese chive (allium tuberosum) root extract for food application," *Int. J. Biol. Macromol.* 150, 595-604. https://doi.org/10.1016/j.ijbiomac.2020.02.078

Sajjadi, M., Nasrollahzadeh, M., Sattari, M. R., Ghafuri, H., and Jaleh, B. (2024). "Sulfonic acid functionalized cellulose-derived (nano)materials: Synthesis and application," *Adv. Colloid Interface Sci.* 328, article 103158. https://doi.org/10.1016/j.cis.2024.103158

Samsalee, N., Meerasri, J., and Sothornvit, R. (2026). "Sustainable packaging film from chitosan reinforced with rice husk cellulose nanocrystals," *Packag. Technol. Sci.* 39(2), 125-136. https://doi.org/10.1002/pts.70025

de Souza, A. G., dos Santos, N. M. A., da Silva Torin, R. F., and dos Santos Rosa, D. (2020). "Synergic antimicrobial properties of carvacrol essential oil and montmorillonite in biodegradable starch films," *Int. J. Biol. Macromol.* 164, 1737-1747. https://doi.org/10.1016/j.ijbiomac.2020.07.226

Sultan, M., Elsayed, H., and Taha, G. (2023). "Potential effect of citrate nanocellulose on barrier, sorption, thermal and mechanical properties of chitosan/arabic gum packaging film," *Food Biosci.* 56, article 103246. https://doi.org/10.1016/j.fbio.2023.103246

Sun, Y., Xu, H., Xie, Y., Ding, K., Liu, Q., Li, Y., Tao, N., Ding, S., and Wang, R. (2025). "Sulfonated cellulose nanocrystalline- and pea protein isolate-mixture stabilizes the citral nanoemulsion to maintain its functional activity for effectively preserving fruits," *Int. J. Biol. Macromol*. 289, article 138725. https://doi.org/10.1016/j.ijbiomac.2024.138725

Takeshita, S., Zhao, S., and Malfait, W. J. (2021). "Transparent, aldehyde-free chitosan aerogel," *Carbohydr. Polym.* 251, article 117089. https://doi.org/10.1016/j.carbpol.2020.117089

Talón, E., Trifkovic, K. T., Nedovic, V. A., Bugarski, B. M., Vargas, M., Chiralt, A., and González-Martínez, C. (2017). "Antioxidant edible films based on chitosan and starch containing polyphenols from thyme extracts," *Carbohydr. Polym.* 157, 1153-1161. https://doi.org/10.1016/j.carbpol.2016.10.080

Tavares, L., Esparza Flores, E. E., Rodrigues, R. C., Hertz, P. F., and Noreña, C. P. Z. (2020). "Effect of deacetylation degree of chitosan on rheological properties and physical chemical characteristics of genipin-crosslinked chitosan beads," *Food Hydrocoll*.106, article 105876. https://doi.org/10.1016/j.foodhyd.2020.105876

Teimouri, S., Morrish, C., Panyoyai, N., Small, D. M., and Kasapis, S. (2019). "Diffusion and relaxation contributions in the release of vitamin B6 from a moving boundary of genipin crosslinked gelatin matrices," *Food Hydrocoll.* 87, 839-846. https://doi.org/10.1016/j.foodhyd.2018.09.015

Tripathi, S., Kumar, P., and Gaikwad, K. K. (2024). "UV- shielding and antioxidant properties of chitosan film impregnated with *Acacia catechu* modified with calcium

carbonate for food packaging," *Int. J. Biol. Macromol.* 257, article 128790. https://doi.org/10.1016/j.ijbiomac.2023.128790

Ulfah, M., Salsabila, A., and Rohmawati, I. (2018). "Characteristics of water solubility and color on edible film from bioselulosa nata nira siwalan with the additional of glycerol," *J. Phys.: Conf. Ser.* 983(1), article 012191. https://doi.org/10.1088/1742-6596/983/1/012191

Vahedikia, N., Garavand, F., Tajeddin, B., Cacciotti, I., Jafari, S. M., Omidi, T., and Zahedi, Z. (2019). "Biodegradable zein film composites reinforced with chitosan nanoparticles and cinnamon essential oil: Physical, mechanical, structural and antimicrobial attributes," *Colloids Surf.* 177, 25-32. https://doi.org/10.1016/j.colsurfb.2019.01.045

Vilarinho, F., Sanches Silva, A., Vaz, M. F., and Farinha, J. P. (2018). "Nanocellulose in green food packaging," *Crit. Rev. Food Sci. Nutr.* 58(9), 1526-1537. https://doi.org/10.1080/10408398.2016.1270254

Wang, X., Huang, D., Ji, L., Yu, Y., Zhu, F., Wang, J., and Liu, C. (2025). "Sulfated chitosan enhances BMP-2-mediated spinal fusion via skeletal stem cell rejuvenation in aging," *Bioact. Mater.* 54, 797-812. https://doi.org/10.1016/j.bioactmat.2025.08.044

Wijesekara, I., Pangestuti, R., and Kim, S.-K. (2011). "Biological activities and potential health benefits of sulfated polysaccharides derived from marine algae," *Carbohydr. Polym.* 84(1), 14-21. https://doi.org/10.1016/j.carbpol.2010.10.062

Wongphan, P., Nampanya, P., Chakpha, W., Promhuad, K., Laorenza, Y., Leelaphiwat, P., Bumbudsanpharoke, N., Sodsai, J., Lorenzo, J. M., and Harnkarnsujarit, N. (2023). "Lesser galangal (*Alpinia officinarum* Hance) essential oil incorporated biodegradable PLA/PBS films as shelf-life extension packaging of cooked rice," *Food Packag. Shelf Life* 37, article 101077. https://doi.org/10.1016/j.fpsl.2023.101077

Wu, D., Lin, Y., Xu, X., Shi, B., Wang, Y., Wang, L., and Song, H. (2026). "A multifunctional zein/tannic acid/stearic acid edible coating with lemongrass essential oil for enhanced preservation of cherry tomatoes," *Int. J. Biol. Macromol.* 345, article 150627. https://doi.org/10.1016/j.ijbiomac.2026.150627

Wu, S., Lu, M., and Wang, S. (2016). "Effect of oligosaccharides derived from laminaria japonica-incorporated pullulan coatings on preservation of cherry tomatoes," *Food Chem.* 199, 296-300. https://doi.org/10.1016/j.foodchem.2015.12.029

Xie, H., Zhang, L., Ouyang, K., Wang, Y., Xiong, H., and Zhao, Q. (2023). "Characterization of rice protein hydrolysate/chitosan composite films and their bioactivities evaluation when incorporating curcumin: Effect of genipin concentration," *Food Bioprocess Technol.* 16(10), 2159-2171. https://doi.org/10.1007/s11947-023-03056-7

Yadav, S., Mehrotra, G. K., and Dutta, P. K. (2021). "Chitosan based ZnO nanoparticles loaded gallic-acid films for active food packaging," *Food Chem.* 334, article 127605. https://doi.org/10.1016/j.foodchem.2020.127605

Yu, J., Xu, S., Goksen, G., Yi, C., and Shao, P. (2023). "Chitosan films plasticized with choline-based deep eutectic solvents: UV shielding, antioxidant, and antibacterial properties," *Food Hydrocoll.* 135, article 108196. https://doi.org/10.1016/j.foodhyd.2022.108196

Zhang, C., Chi, W., Meng, F., and Wang, L. (2021). "Fabricating an anti-shrinking κ-carrageenan/sodium carboxymethyl starch film by incorporating carboxylated cellulose nanofibrils for fruit preservation," *Int. J. Biol. Macromol.* 191, 706-713.

https://doi.org/10.1016/j.ijbiomac.2021.09.134

Zhang, K., Qian, Y., Wang, H., Fan, L., Huang, C., Yin, A., and Mo, X. (2010). "Genipin-crosslinked silk fibroin/hydroxybutyl chitosan nanofibrous scaffolds for tissue-engineering application," *J. Biomed. Mater. Res., Part A.* 95(3), 870-881. https://doi.org/10.1002/jbm.a.32895

Zhang, W., Shu, C., Chen, Q., Cao, J., and Jiang, W. (2019). "The multi-layer film system improved the release and retention properties of cinnamon essential oil and its application as coating in inhibition to penicillium expansion of apple fruit," *Food Chem.* 299, article 125109. https://doi.org/10.1016/j.foodchem.2019.125109

Zhang, Y., Tang, H., Lei, D., Zhao, B., Zhou, X., Yao, W., Fan, J., Lin, Y., Chen, Q., Wang, Y., Li, M., He, W., Luo, Y., Wang, X., Tang, H., and Zhang, Y. (2023). "Exogenous melatonin maintains postharvest quality in kiwiberry fruit by regulating sugar metabolism during cold storage," *LWT* 174, article 114385. https://doi.org/10.1016/j.lwt.2022.114385

Zhang, Z., Li, X.-M., Guo, Y., Wang, H., Li, Z., and Lin, H. (2025). "Insight into the anti-allergic impacts of fucoidan from *Gracilaria lemaneiformis* in mitigating allergic reactions induced by shrimp tropomyosin via regulating Th1/TH2 cytokines and T cell subsets," *Int. J. Biol. Macromol.* 299, article 140228. https://10.1016/j.ijbiomac.2025.140228

Zhu, Z., Yu, M., Ren, R., Wang, H., and Kong, B. (2024). "Thymol incorporation within chitosan/polyethylene oxide nanofibers by concurrent coaxial electrospinning and in-situ crosslinking from core-out for active antibacterial packaging," *Carbohydr. Polym.* 323, article 121381. https://doi.org/10.1016/j.carbpol.2023.121381

Article submitted: January 28, 2026; Peer review completed: February 28, 2026; Revised version received and accepted: March 23, 2026; Published: April 27, 2026.
DOI: 10.15376/biores.21.2.5205-5227